Analysis of Acoustic Emission Energy Distribution and Avalanche Dynamics of Sandstone with Different Particle Sizes

Jianguo Zhang, Yingwei Wang, and Zepeng Wang*

Read Online

ACCESS | Metrics & More | Article Recommendations

ABSTRACT: The mechanical properties of sandstone have an important impact on the stability of the coal mine roof and floor, sandstone gas mining, and underground engineering safety. In order to study the critical characteristics on the failure process of sandstone with different particle sizes under uniaxial compression conditions, avalanche dynamics theory and a critical model are used to analyze the distribution of acoustic emission (AE) parameters, and the maximum likelihood estimation is used to accurately estimate the critical parameters. The results showed that the AE phenomenon of sandstone can be divided into four stages: initial compaction period, quiet period, crack stable growth period and outbreak period. During the process of compression failure, the larger the particle size is, the more seriously the sandstone is damaged. The AE energy probability density distribution follows single power-law distribution, and the AE energy critical exponent is 1.20 and follows the characteristics of scale-free regarding the power-law distribution on the particle sizes. When the stress runs up to 90% of peak stress, the bifurcation ratio increases sharply and shows the characteristics of the critical state. The waiting time and the avalanche size distribution follow double power-law distribution, and the inflection points are 0.03 and 37. Before and after the inflection point, the waiting time critical exponent and the avalanche size critical exponent are 1.90, 0.40 and 2.40, 1.60. This shows that the dynamic evolution process of sandstone under uniaxial compression condition can be characterized well by the fiber bundle model.
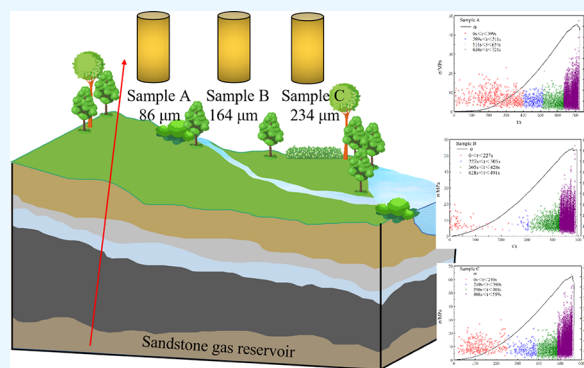
1. INTRODUCTION

With the increasing global demand for energy, especially clean energy, the exploitation of unconventional natural gas (EUG) has become one of the important energy supplies.[1] The EUG represented by shale gas and sandstone gas largely determines the future of clean energy development. Although the application prospects of unconventional natural gas are very good, the EUG has been restricted by problems such as low pressure, low porosity, and low permeability.[2−4] In order to solve these problems, fracturing technology has been widely used in EUG.[2−4] In the process of fracturing and antireflection, the mechanical properties of reservoir rocks have an important impact on the effect of fracturing and antireflection.[5] Therefore, studying the deformation and failure mechanism of sandstone under stress is of great significance to the EUG.

As an important engineering object, the fracture damage characteristics of rock have been paid much attention by the scientific and engineering circles. However, due to its discontinuity, heterogeneity, nonlinearity, and anisotropy, it is a great challenge to study its fracture damage characteristics.[6] In recent years, many researchers began to use the phase transition and critical theory in statistical physics to study this issue and achieved a series of results.[7−13] The research shows

that the failure evolution process of rock is critical, which is a generalized second-order phase transition process.[7−13] This criticality of rock is represented by the statistical scale-free distribution on different scales when subjected to external action, and the scale-free distribution law can be characterized by the critical index, and this index can be used to predict some mechanical parameters of the same kind but different individuals.[10] Recent studies have shown that by using the mean field model, the power distribution index of breaking noise can be used to predict the stress of materials under compression.[11] This allows us to predict and analyze the failure stress by using the critical index through the breaking noise before the material has reached macrofailure. Therefore, it is very important to obtain a high-precision critical index.[12] The destructive noise mentioned here refers to the response

physical quantity of sudden change of materials under external action, also known as an avalanche event.[13] In 1994, Eduard[14] first introduced avalanche dynamics into the research field of material damage, which promoted the related research of condensed matter physics. Acoustic emission (AE) is a kind of avalanche event, and the statistical analysis of AE signals in the process of rock deformation and failure can help us understand the relevant mechanism of rock failure. Jiang[15] studied the degradation effect of supercritical carbon dioxide on sandstone, found that supercritical carbon dioxide reduced the strength of sandstone, and characterized the damage of sandstone by using the probability statistical density of acoustic emission energy for the first time. At present, the research on the acoustic emission phenomenon in the process of sandstone failure mostly focuses on the basic information such as acoustic emission amplitude and ring counting, while the research on the critical characteristics in the process of failure is rarely reported. Therefore, the study on the critical characteristics in the process of sandstone failure under different particle sizes is helpful to understand the failure characteristics of sandstone and provide theoretical support for engineering safety.

In this paper, the mechanics and AE data of sandstone with different particle sizes during uniaxial compression are quantitatively analyzed by using avalanche dynamics theory and critical model. The distribution laws of AE energy, avalanche size, and waiting time of sandstone with different particle sizes are studied, and the critical characteristics and critical power distribution laws of sandstone during uniaxial compression failure are obtained. The maximum likelihood estimation method is used to accurately estimate the power distribution index, so as to reveal the evolution mechanism in the process of rock failure. The research results provide theoretical support for geotechnical engineering applications such as EUG.

2. MATERIALS AND METHODS

2.1. Sample Preparation. The rock samples used in the test were collected from Chongqing and surrounding areas. Through the mineral composition analysis and particle size analysis of the collected rock samples,[16] sandstone with the same mineral composition and cement but different particle size is selected. Finally, three kinds of sandstones with different grain sizes are selected and divided into three groups: Group A, Group B, and Group C. The median particle sizes are 86 μm, 164 μm, and 234 μm, respectively.

In order to ensure that the test results have small dispersion, the rock specimens used in the tests were drilled from the same rock mass with good integrity and homogeneity, respectively. The specimens were processed in strict accordance with the method recommended by the International Society of Rock Mechanics, and the specimens were cylinders of ϕ50 mm × 100 mm with smooth surfaces and no obvious defects, and the ends were smoothed, and the nonparallelism was controlled within ±0.02 mm.

2.2. Mechanical Test. The test loading equipment adopts the American MTS815 rock hydraulic servo-mechanical system as shown in Figure 1. The equipment has a maximum axial loading load of 2,800 kN and is automatically controlled by a fully digital computer, which can be used for force, displacement, axial strain and other loading methods, and high-speed data acquisition. The equipment for AE monitoring uses the PCI-II AE detector produced by PAC, an American acoustic physics company. The test and analysis system has the
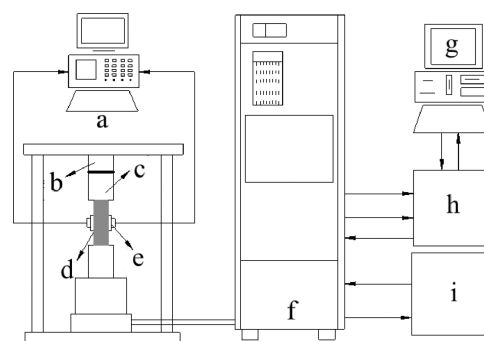
Figure 1. Schematic diagram of test system (a. PCI-II AE detector; b. Load sensor; c. Loading device; d. Rock specimen; e. AE probe; f. MTS servo supercharger; g. Computer control system; h. MTS controller; i. MTS hydraulic source.)

technical characteristics of AE characteristic parameters and waveform acquisition at the same time, anti-interference ability, and noise exclusion ability.

In order to obtain the mechanical and AE data of sandstone in different stages of the whole stress−strain process, three groups of sandstone specimens were subjected to uniaxial compression AE tests. During the test, AE monitoring and load loading are carried out at the same time, and the mechanical and AE data in the process of uniaxial compression deformation and failure are collected.

The test steps are as follows: first, two AE probes are symmetrically arranged in the middle of the rock specimen. In order to ensure close contact between the AE probe and the rock specimen, the AE probe and the rock specimen are coupled with butter and tied tightly with bandage. Then the rock specimen is placed according to the specified requirements. The laboratory is kept quiet, but in order to reduce the impact of indoor noise on the AE test, 40 dB is taken as the AE threshold in the test. The AE system was tested to ensure proper signal transmission, and then an axial load was applied at a loading rate of 0.1 mm/min until the rock specimen was damaged.

3. RESULTS AND DISCUSSION

3.1. Characteristics of AE Energy. AE is an instantaneous elastic wave generated by the rapid release of local strain energy in the material.[17] It comes from the deformation and damage inside the material or structure. The generation and development of internal cracks during the fracture of brittle rock is a good AE signal source. Therefore, as an associated phenomenon in the process of rock failure, AE contains a lot of information about the internal failure process of rock.[17] As shown in Figure 2, the stress time AE energy relationship of sandstone with different particle sizes in the process of uniaxial compression failure is shown.

From the figure, we can see that the change law of AE energy of sandstone is roughly the same under the three particle sizes. Combined with the stress change, the whole evolution process can be divided into four stages: primary crack compaction stage, calm stage, crack stable development stage, and failure stage. Combined with Table 1, we can find that in the compaction stage of the primary crack, there are many AE energy signals and low energy values, which are basically concentrated in the range of $10^0 - 10^4$ aJ, mainly from the closure of primary cracks in rock. In the quiet stage, the AE energy signal decreases and the energy peak decreases, mainly
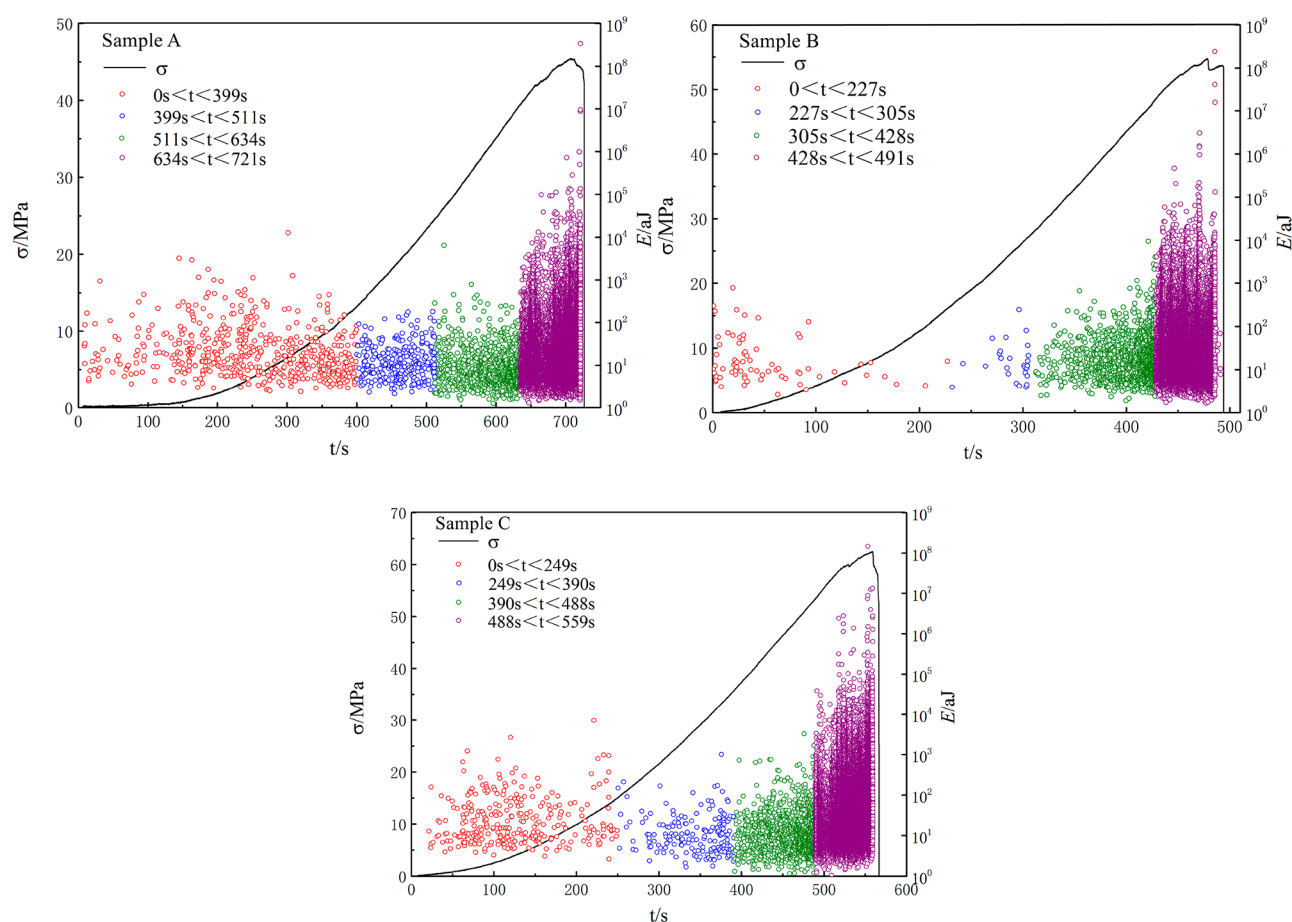
Figure 2. Stress-time-AE energy diagram of all studied samples.

Table 1. AE Energy Parameters of Each Stress Level

Group	Time/s	Stress/MPa	AE energy number	AE Energy/aJ	Proportion/%	Cumulative AE energy/aJ
A	0−399	0−13.2	525	10^0−10^4	1.86	5.04×10^5
	399−511	13.2−24.5	350	10^0−10^2	1.24	1.09×10^5
	511−634	24.5−39.4	1001	10^0−10^3	3.55	2.38×10^5
	634−721	39.4−45.4	26297	10^0−10^8	93.34	3.63×10^8
	0−721	0−45.4	28173	10^0−10^8	100	3.63×10^8
B	0−227	0−16.1	73	10^0−10^3	0.26	3.16×10^3
	227−305	16.1−27.2	26	10^0−10^2	0.09	7.24×10^2
	305−428	27.2−48.5	1400	10^0−10^4	5.04	7.02×10^5
	428−491	48.5−54.8	26303	10^0−10^8	94.61	3.14×10^8
	0−491	0−54.8	27802	10^0−10^8	100	3.14×10^8
C	0−249	0−15.0	302	10^0−10^4	0.78	2.84×10^5
	249−390	15.0−35.6	182	10^0−10^2	0.47	6.69×10^3
	390−488	35.6−53.1	1292	10^0−10^4	3.31	3.74×10^5
	488−559	53.1−62.5	37182	10^0−10^8	95.44	2.33×10^8
	0−559	0−62.5	38958	10^0−10^8	100	2.33×10^8

in the range of 10^0−10^2 aJ. This is because at this stage, the primary crack has basically been completely closed, while the new crack has not yet occurred. In the stable development stage of the crack, the AE energy signal increases, but the energy value changes little, and it is mainly concentrated in the range of 10^0−10^4 aJ, which is caused by new cracks in the rock with the continuous increase of load. In the failure stage, the AE signal increases sharply, and the energy value jumps by multiple orders of magnitude, mainly in the range of 10^0−10^8 aJ. At this stage, a large number of new cracks in the rock are

generated and continue to fuse and expand until the rock specimen is damaged.

Combined with Table 1 and Figure 3, we can find that with the increase of particle size, the cumulative AE energy of sandstone in the whole failure evolution process decreases, from 3.63×10^8 aJ reduced to 2.33×10^8 aJ, but the energy number increased from 28173 times to 38958 times, and the proportion of the failure stage also increased from 93.34% to 95.44%, which shows that with the larger particle size, the number of AE events, i.e., microcracks, of sandstone in the
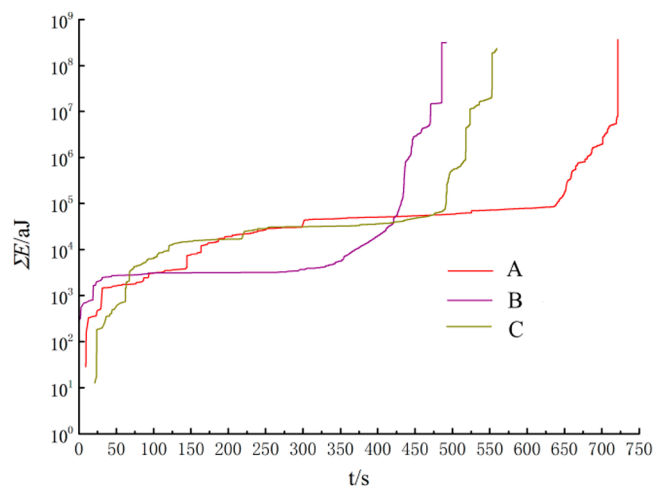
Figure 3. Curves of cumulative AE energy of samples A, B, and C.

failure stage increases, but the energy value decreases. However, it can be seen from Figure 2 that in the failure stage, the number of AE energy with high energy value increases with the increase of particle size. Combined with the failure phenomenon observed in the test: the larger the particle size, the more severe the failure of rock specimen in the test,

the more fragments and macro cracks. This shows that the larger the particle size, the more microcracks and the lower the energy value in the failure stage of sandstone, but the more macrocracks formed by fusion and expansion, and the more severe the rock failure. Therefore, we can speculate that the larger the particle size, the more it can promote the propagation and fusion of microcracks into macrocracks.

3.2. Power Law Distribution of AE Energy Probability Density. The AE energy is obtained by the acquisition system through the square integral of the signal voltage, and the calculation formula is[18]

$$E = \int_{t_i}^{t_j} U^2(t)d_t/R \qquad (1)$$

where t_i and t_j represent the starting and ending time points of AE events respectively, R represents the group value in the acquisition workstation, and the event duration $T = t_j - t_i$.

Each energy value of AE energy is independent, and they constitute the AE energy set. For this discrete sample set, the probability density power-law distribution function can be expressed as[9,18–21]

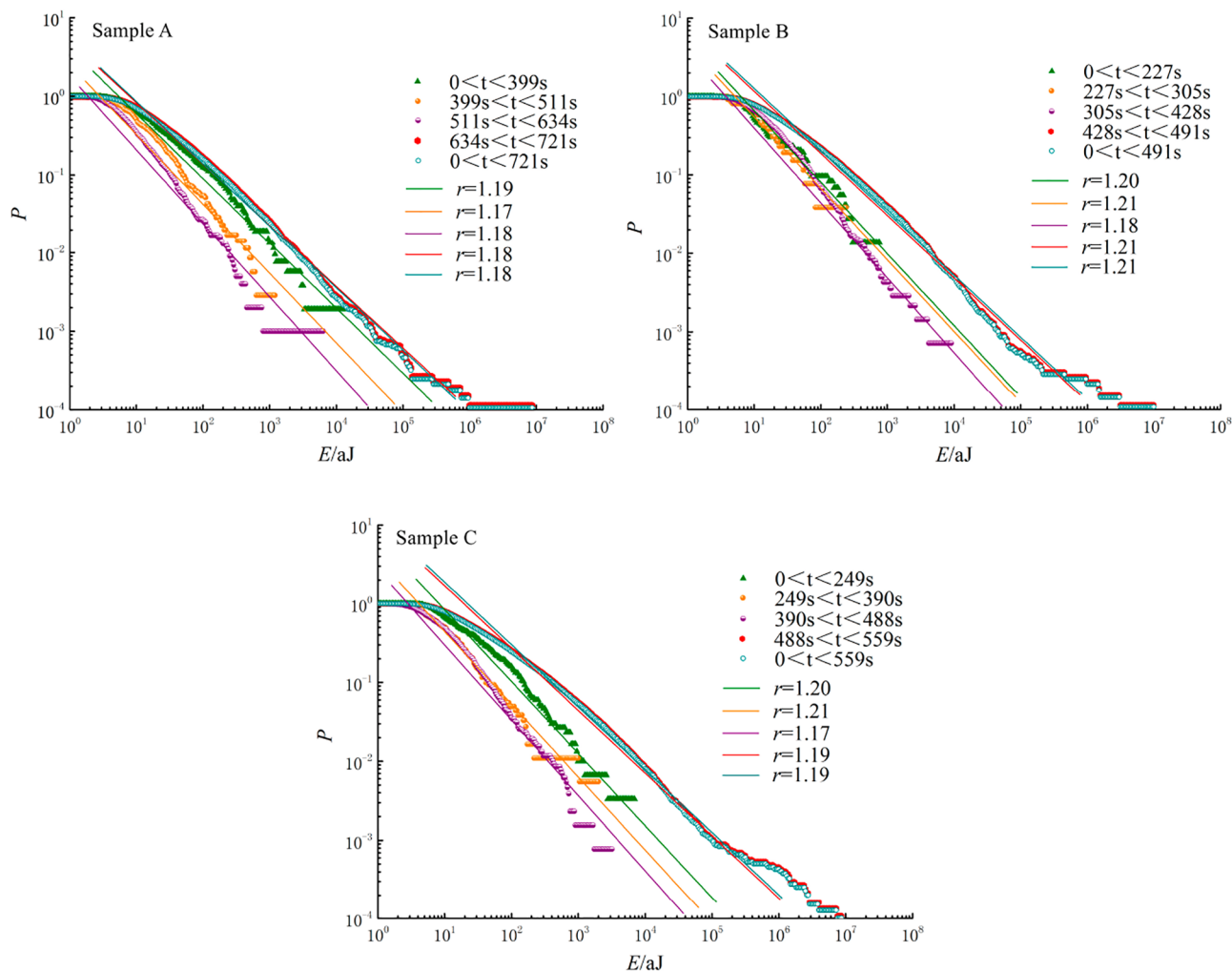$$p(x) = \frac{x^{-r}}{\tau(r, x_{min})} \qquad (2)$$

Figure 4. Distribution of AE energy probability density of all studied samples.

Where r is the power critical index representing the whole probability density distribution, τ represents the Hurwitzzeta function, and x_{min} is the standardized parameter.

After obtaining the probability density distribution curve of AE energy, we can obtain its critical index r by the fitting method, but the traditional fitting method is greatly affected by artificial division, and the result is inaccurate. Therefore, this paper uses the maximum likelihood estimation method to accurately estimate the power critical index r. Equation for maximum likelihood estimation of critical index r can be expressed as[9,18−21]

$$\frac{\tau'(r', x_{min})}{\tau(r', x_{min})} = -\frac{1}{n} \sum_{i=1}^{n} \ln x_i \tag{3}$$

Equation 3 is too complicated and difficult to solve. For the maximum likelihood estimation of this discrete variable, when $x_{min} \geq 6$, the following simple approximate formula can be used to replace it:[9,18−21]

$$r' = 1 + n \left[\sum_{i=1}^{n} \ln \frac{x_i}{x_{min} - \frac{1}{2}} \right]^{-1} \tag{4}$$

where x_i, $i = 1, 2, 3, \cdots, N$ are all observations satisfying the inequality $x_i \geq x_{min}$.

In order to evaluate the deviation of the r' corresponding to the energy sample set n, the standard deviation of the power value can be approximately estimated by using the second derivative of the maximum likelihood function:

$$\Delta_{r'} = \left\{ \frac{\partial^2 \ln \nu}{\partial r'^2} \bigg|_{max} \right\}^{-1/2} \tag{5}$$

Through calculation simplification, the following formula[9,18−21] can be used instead:

$$\Delta_{r'} = \frac{r' - 1}{\sqrt{n}} \tag{6}$$

Figure 4 shows the distribution curve of AE energy density of sandstone with different particle sizes in the process of uniaxial compression failure. Through comparison, we can find that under the three particle sizes, the probability density distribution of AE energy of sandstone in different stages of the uniaxial compression failure process presents a relatively good linear distribution relationship as a whole. It shows that the energy distribution of sandstone in uniaxial compression process obeys the single power law. As shown in Table 2, the distribution trend of sandstone with three particle sizes in the four stages of failure evolution process is similar to that in the whole process, and the critical index r is around 1.20 ± 0.02, which also proves the scale-free power distribution, indicating that the particle size has little effect on the probability density distribution of AE energy of sandstone. Due to the similarity between the whole and the part, we can also extract the AE energy signal before the rock specimen is completely destroyed, accurately estimate the critical index r by using the maximum likelihood estimation method, and then effectively predict the energy in the failure stage. Using this theory, we can make use of it in practical engineering, It is possible to predict the energy of rock failure.

Using eqs 4 and 6, we can calculate the distribution of critical index r and its error bar of sandstone in the whole

Table 2. AE Energy Critical Index of Each Stress Level

Group	Time/s	AE energy critical index r
A	0−399	1.19
	399−511	1.17
	511−634	1.18
	634−721	1.18
	0−721	1.18
B	0−227	1.20
	227−305	1.21
	305−428	1.18
	428−491	1.21
	0−491	1.21
C	0−249	1.20
	249−390	1.21
	390−488	1.17
	488−559	1.19
	0−559	1.19

failure evolution process. As shown in Figure 5, we can find that the critical index is relatively stable and concentrated in
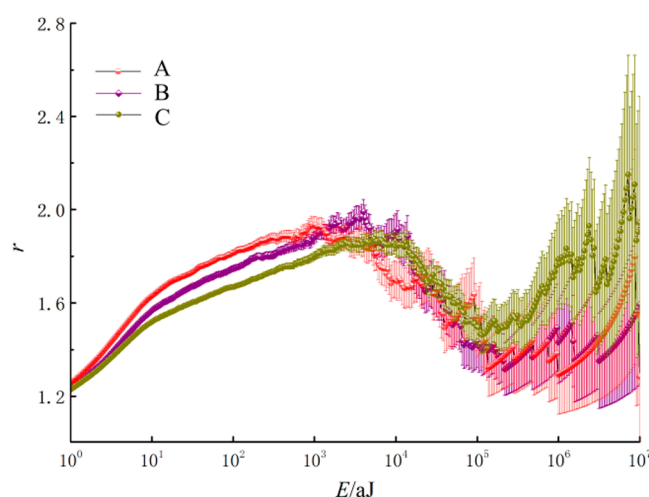

Figure 5. Distribution of exponent r and error bar of Samples A, B, and C.

the low-energy region, while there is disorder in the high-energy region, mainly because the number of high-energy AE events is small and discrete. Therefore, there is a large error and disorder in the phase. In addition, we can find that particle size has an obvious influence on the distribution of critical index R in the whole process of sandstone failure evolution, and the influence law is just the opposite in high-energy area and low-energy area, that is, before and after the peak of critical index. In general, most low-energy AE events are mainly caused by the development, closure, and propagation of independent and uncorrelated cracks. When these independent cracks fuse and fracture to produce macrocracks, they often produce high-energy AE events. We can infer from this point that the particle size will have significantly different effects on the two AE events, and the influence mechanism needs to be further studied.

3.3. Critical Characteristic Analysis Based on the Bifurcation Rate. Among many research methods of statistical mechanics, the fiber bundle model is a simulation tool with simple principle but can reflect the fracture evolution process of the materials. Peirce[22] first proposed that there are

several fibers between two planes (the constitutive relations of these fibers themselves can be diverse and the strength of fibers can be different, which provides a basis for the study of heterogeneity), They jointly bear the external force **F** applied to the system. When the weakest fiber in the system breaks due to the external force, the stress borne by the remaining fibers will be shared by the remaining fibers according to certain rules. After the remaining fibers have this stress increment, they may reach a new balance or continue to break beyond their own strength, resulting in a chain effect, until the macro-fracture of the material is reached. This chain effect is called the avalanche effect, and the size of the chain effect is called the avalanche size.[23] Therefore, the method of combining a fiber bundle model with AE parameters to study material fracture dynamics is called a new research hotspot.

The research shows that[24,25] the fracture instability of the solid meets the characteristics of the second-order phase transition; that is, there is a continuous critical variable. When the system reaches the critical point from no external excitation to variable external excitation, this variable continuously changes from 1 to 0. We define the bifurcation rate to describe the behavior characteristics of each avalanche event when the external excitation is close to the critical withstand value. Its size has the following functional relationship with the number of avalanche events (i.e., the number of fiber breaks):

$$\xi = \frac{\langle Z \rangle - 1}{\langle Z \rangle} \tag{7}$$

We can regard the rock fracture process as the evolution process of fiber branch fracture so as to calculate the bifurcation rate ξ. In this bifurcation process, each node will induce the next n new bifurcations. The average number of these new bifurcations $\langle n \rangle$ is called the bifurcation rate. Assuming that there is a n_k branch at the kth bifurcation and it ends after $k_{\max}$ bifurcation, the bifurcation rate ξ can be expressed as

$$\xi = 1 - \frac{n_0}{\sum_{k=0}^{k_{\max}} n_k} \tag{8}$$

In the fiber bundle model, it is assumed that $n_0 = 1$; n_k represents the sum of all nodes in the bifurcation process, which is equal to the average number of fracture events in the fracture process.

As shown in Figure 6, the evolution relationship between branching rate and stress of sandstone with different grain sizes during uniaxial compression failure is shown. From the figure, we can see that when the stress of the sandstone specimen is less than 90% of the peak stress, the bifurcation rate is very small, close to 0, and changes little. When the stress reaches 90% of the peak stress, the bifurcation rate increases sharply until the specimen is damaged. This is consistent with the simulation results of the fiber bundle model based on mean field theory by Moreno et al., which further proves the feasibility of using mean field theory model in the sandstone uniaxial compression test.

3.4. Statistical Distribution of Time Difference before and after Critical Point. The time difference between adjacent events of AE is called the waiting time, represented by δ:[26]

$$\delta_j = t_j - t_{j-1} \tag{9}$$
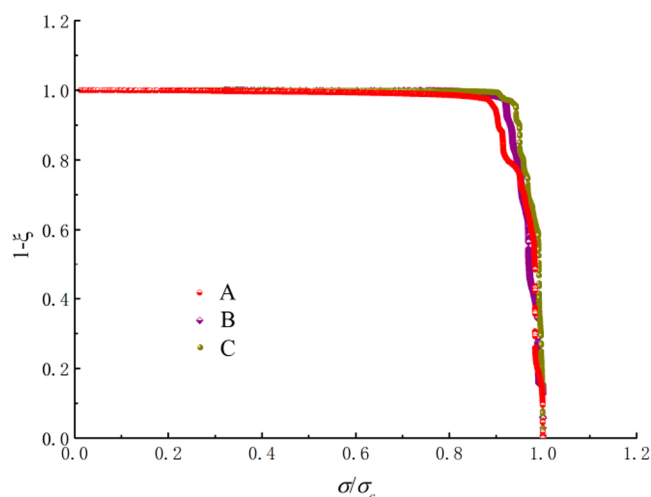
Figure 6. Relationship between branching rate and stress of Sample A, B and C.

j represents an event greater than the custom minimum energy threshold E^*.

Using the data processing software Igor Pro to process the waiting time series of sandstone with different particle sizes in the process of uniaxial compression failure, the distribution function $D_{E,R}(\delta)$ of waiting time δ is obtained to characterize.

As shown in Figure 7, the distribution curve of waiting time of sandstone with different grain sizes in the process of uniaxial
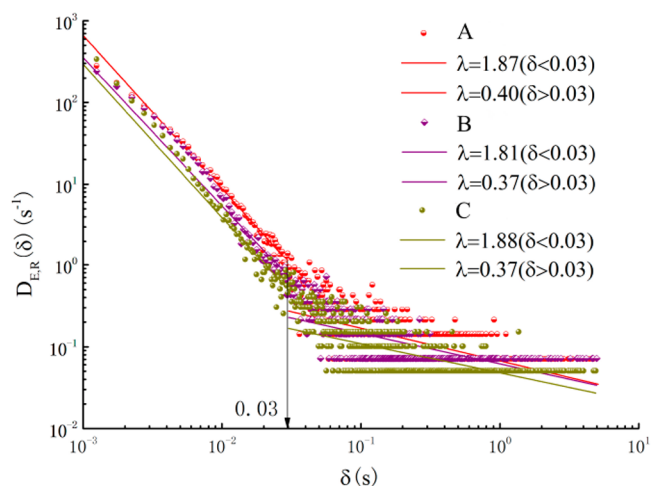
Figure 7. Distribution of AE waiting-time probability density of Samples A, B, and C.

compression failure is shown. From the figure, we can see that the distribution law of waiting time is roughly the same under the three grain sizes, the difference is small, and both meet the double power law, showing an inflection point near $\delta = 0.03$ s. Before and after the inflection point, the power distribution indexes of waiting time of Groups A, B, and C are 1.87, 1.81, 1.88 ($\delta < 0.03$), 0.40, 0.37, and 0.37 ($\delta > 0.03$). It can be seen that there is little difference between the three groups, which also proves that the waiting time of sandstone meets the power scale-free distribution in time. Using this law, we can judge the probability of time interval between adjacent AE events in the process of sandstone failure. From the figure, we can also find that when $\delta < 0.03$, the distribution of waiting time is relatively concentrated, while when $\delta > 0.03$, the distribution of waiting

time is relatively discrete. From Table 1, we know that most AE events occur before and after the critical point, and these AE signals are basically new cracks and fissures, which develop and expand rapidly. Therefore, the time difference between adjacent AE events after the critical state is very small, basically less than 0.03, with high frequency, so they are relatively concentrated. The AE signal $\delta > 0.03$ is mainly caused by the closure of the primary crack; the waiting time range is relatively large and the frequency is not high, so it is relatively discrete.

3.5. Probability Distribution Analysis of Sandstone Avalanche Size. According to Pradhan et al. and Hemmer et al.,[22,27−29] for the fiber bundle model, the avalanche size distribution satisfies the following relationship:

$$\frac{D(\Delta)}{N} = \frac{\Delta^{\Delta-1} e^{-\Delta}}{\Delta!} \int_0^{x_c} p(x)\Gamma(x)\, dx$$
$$= \frac{\Delta^{\Delta-1} e^{-\Delta}}{\Delta!} \int_0^{x_c} p(x) r(x)[1 - r(x)]^{\Delta-1} \exp[\Delta r(x)]\, dx \tag{10}$$

where $r(x) = \frac{x p(x)}{1 - P(x)}$ represents the average number of broken fibers, $\Gamma(x)$ represents the probability of breaking the first fiber when the avalanche size is Δ, and x represents the fiber strength.

When x reaches the critical threshold x_c, the following equation holds

$$1 - P(x_C) - x_c p(x_c) = 0 \tag{11}$$

Here, $r(x_c) = 1$; therefore

$$(1 - r)^\Delta e^{\Delta r} \approx \exp[-\Delta r(x)^2/2] \tag{12}$$

Since $r(x) \approx r'(x_c)(x - x_c)$, therefore

$$\frac{D(\Delta)}{N} = \frac{\Delta^{\Delta-1} e^{-\Delta}}{\Delta!} \int_0^{x_c} p(x)\Gamma(x)\, dx$$
$$= \frac{\Delta^{\Delta-2} e^{-\Delta} p(x_c)}{|(x_c) r'|\Delta!}[e^{-\Delta r'(x_c)^2(x-x_c)^2/2}]_{x_0}^{x_c}$$
$$= \frac{\Delta^{\Delta-2} e^{-\Delta}}{\Delta!}\frac{p(x_c)}{|(x_c)r'|}[1 - e^{-\Delta/\Delta_c}] \tag{13}$$

where $\Delta_c = \frac{2}{r'(x_c)^2(x_c - x_0)^2}$

Stirling formula $\Delta! \approx \sqrt{2\pi}\,\Delta^{\Delta+1/2} e^{-\Delta}$ is introduced to simplify formula 13 as follows:

$$\frac{D(\Delta)}{N} = C\Delta^{-5/2}(1 - e^{-\Delta/\Delta_c}) \tag{14}$$

where $C = 2\pi^{-1/2} p(x_c)/|r'\, x_c|$.

From the cumulative probability distribution diagram of avalanche size in Figure 8, we can find that under the three particle sizes, the change law of probability distribution of avalanche size is the same, which has experienced a linear increase to the final trend. However, we can clearly find that the larger the particle size, the higher the proportion of low avalanche size, and the corresponding proportion of high avalanche size is relatively reduced, which shows that the particle size has a significant impact on the avalanche size in the rock avalanche effect.

From the avalanche size distribution diagram in Figure 9, we can see that the avalanche size distribution under the three particle sizes well follows the bilinear distribution relationship,
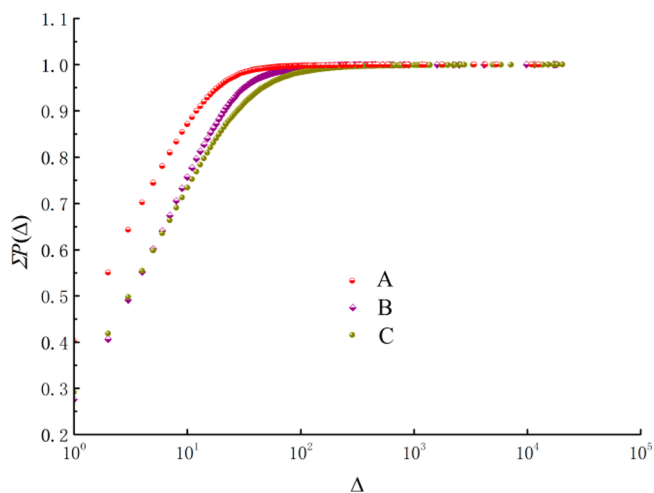
Figure 8. Distribution of cumulative avalanche size probability of Samples A, B, and C.
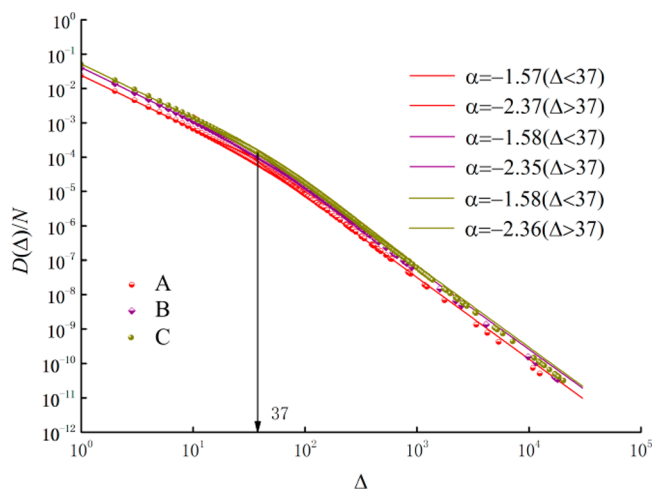
Figure 9. Distribution of avalanche size of Samples A, B, and C.

indicating that the avalanche size distribution meets the double power law distribution, and there is an inflection point near $\Delta = 37$. Before and after the inflection point, the critical indexes are 1.57, 1.58, 1.58 and 2.37, 2.35, 2.36, with little difference. This shows that the particle size has little effect on the critical index of avalanche size distribution, which confirms the scale-free characteristics of critical characteristics. It is also proved that the fiber bundle model can be used to quantitatively describe the dynamic evolution process of rock failure.

4. CONCLUSIONS

Using the critical theory, this paper analyzes and studies the acoustic emission energy data of sandstone with different particle sizes during uniaxial compression failure, analyzes the influence of particle sizes on the failure characteristics of sandstone, and obtains the following conclusions:

1. The uniaxial compression failure process of sandstone can be divided into four stages: primary crack compaction stage, calm stage, crack stable propagation stage, and failure stage. The larger the particle size is, the more intense the failure of sandstone is.

2. The probability density distribution of AE energy of sandstone under different particle size conditions obeys

the single power law distribution, the critical index r is 1.20, and follows the power-law scale-free distribution on particle size.

3. When the stress reaches about 90% of the peak stress, the bifurcation rate increases sharply and shows good critical state characteristics. The waiting time and avalanche size distribution obey the double power law distribution and have inflection points, which are $\delta = 0.03$ and $\Delta = 37$, respectively. The critical indexes before and after the inflection point are 1.90, 0.40, 1.60, and 2.40, respectively. It is also proved that the fiber bundle model can well characterize the dynamic evolution process of sandstone uniaxial compression.

The above research results provide theoretical support for further understanding the failure characteristics of sandstone. However, under engineering conditions, sandstone is in a triaxial stress state and is affected by multiple factors such as temperature, water, and gas. However, our current research has not yet paid attention, which is our future research direction.

■ AUTHOR INFORMATION

Corresponding Author

Zepeng Wang − *College of Safety Science and Engineering, Henan Polytechnic University, Jiaozuo 454000, China;* ⊚ orcid.org/0000-0003-4141-6398; Email: zpwang@ cqu.edu.cn

Authors

Jianguo Zhang − *State Key Laboratory of Coking Coal Exploitation and Comprehensive Utilization, Pingdingshan 467000, China*

Yingwei Wang − *State Key Laboratory of Coking Coal Exploitation and Comprehensive Utilization, Pingdingshan 467000, China*

Complete contact information is available at: https://pubs.acs.org/10.1021/acsomega.3c01024

Notes

The authors declare no competing financial interest.

■ REFERENCES

(1) Lu, Y. Y.; Zhang, H. D.; Zhou, Z.; Ge, Z. L.; Chen, C. J.; Hou, Y. D.; Ye, M. L. Current Status and Effective Suggestions for Efficient Exploitation of Coalbed Methane in China: A Review. *Energy & Fuels.* **2021**, *35* (11), 9102−9123.

(2) Wang, Z.; Ge, Z.; Li, R.; Zhou, Z.; Hou, Y.; Zhang, H. Coupling effect of temperature, gas, and viscoelastic surfactant fracturing fluid on the microstructure and its fractal characteristics of deep coal. *Energy & Fuels.* **2021**, *35* (23), 19423−19436.

(3) Zepeng, W.; Zhaolong, G.; Ruihui, L.; Xianfeng, L.; Haoming, W.; Shihui, G. Effects of acid- based fracturing fluids with variable hydrochloric acid contents on the microstructure of bituminous coal: An experimental study. *Energy.* **2022**, *244*, 122621.

(4) Zhaolong, G.; Zepeng, W.; Jinhong, H.; Yingwei, W.; Zhe, Z.; Ruihui, L. Effect of different types of fracturing fluid on the microstructure of anthracite: an experimental study. *Energy Sources, Part A: Recovery, Utilization, and Environmental Effects.* **2021**, 1−15.

(5) Han, C.; Jiang, Z. X.; Han, M.; Wu, M. H.; Lin, W. The lithofacies and reservoir characteristics of the Upper Ordovician and Lower Silurian black shale in the Southern Sichuan Basin and its periphery, China. *Marine and Petroleum Geology.* **2016**, *75*, 181−191.

(6) Zheng, Y. R.; Liu, X. H. The problems of modern nonlinear science and rock mechanics. *Chinese Journal of Geotechnical Engineering.* **1996**, *18* (1), 98−100.

(7) Bonamy, D.; Bouchaud, E. Failure of heterogeneous materials: A dynamic phase transition? *Physics Reports.* **2011**, *498* (1), 1−44.

(8) Friedman, N.; Jennings, A. T.; Tsekenis, G.; Kim, J. Y.; Tao, M. L.; Uhl, J. T.; Greer, J. R.; Dahmen, K. A. Statistics of dislocation slip avalanches in nanosized single crystals show tuned critical behavior predicted by a simple mean field model. *Phys. Rev. Lett.* **2012**, *109* (9), 6709−6717.

(9) Jiang, D. Y.; Xie, K. N.; Jiang, X.; Chen, J.; Yuan, X. Statistical analysis of acoustic emission energy distribution during uniaxial compression of shale. *Chinese Journal of Rock Mechanics and Engineering.* **2016**, *35* (S2), 3822−3828.

(10) Moreno, Y.; Gomez, J. B.; Pacheco, A. F. Fracture and second-order phase transitions. *Phys. Rev. Lett.* **2000**, *85* (14), 2865−2868.

(11) Dahmen, K. A.; Ben-zion, Y.; Uhl, J. T. Micromechanical model for deformation in solids with universal predictions for stress-strain curves and slip avalanches. *Phys. Rev. Lett.* **2009**, *102* (17), 175501−175505.

(12) Salje, E. K. H.; Dahmen, K. A. Crackling noise in disordered materials. *Annual Review of Condensed Matter Physics.* **2014**, *5* (1), 233−254.

(13) Sethna, J. P.; Dahmen, K. A.; Myers, C. R. Crackling noise. *Nature* **2001**, *410*, 242−250.

(14) Vives, E.; Ortin, J.; Manosa, L.; Rafols, I.; Perez-Magrane, R.; Planes, A. Distributions of avalanches in martensitic transformations. *Phys. Rev. Lett.* **1994**, *72*, 1694.

(15) Jiang, X.; Qian, K.; Wang, X. S.; Gao, S. X.; Xie, K. N. Effect of supercritical CO_2 on mechanical properties of sandstone using acoustic emission and NMR. *Rock and Soil Mechanics.* **2018**, *39* (4), 1355−1361.

(16) Cai, X. S.; Su, M. X.; Shen, J. Q.*Particle size measurement technology and application*; Chemical Industry Press: Beijing, 2010.

(17) Qin, S. Q.; Li, Z. D.; Zhang, Z. Y.*An introduction to acoustic emission technology on rocks*; Southwest Jiaotong University Press: Chengdu, 1993.

(18) Clauset, A.; Shalizi, C. R.; Newman, M. E. J. Power-law distributions in empirical data. *Society for Industrial and Applied Mathematics.* **2009**, *51* (4), 661−703.

(19) Jiang, D. Y.; He, Y.; Ouyang, Z. H.; Pan, P. Z.; Wang, X. S.; Xie, K. N.; Jiang, X. Acoustic emission energy statistical properties of sandstone during uniaxial creep and its fracture surfaces morphology. *Journal of china coal society.* **2017**, *42* (06), 1436−1442.

(20) Xie, K. N.; Jiang, D. Y.; Jiang, X.; Chen, J.; Wang, J. Y.; Yuan, X.; Zhou, J. P. Energy distribution and criticality characteristics analysis of shale Brazilian splitting test. *Journal of china coal society* **2017**, *42* (03), 613−620.

(21) Castillo-Villa, P. O.; Baro, J.; Planes, A.; Salje, E. K. H.; Sellappan, P.; Kriven, W. M.; Vives, E. Crackling noise during failure of alumina under compression: the effect of porosity. *Journal of Physics: Condensed Matter.* **2013**, *25*, 292202−292211.

(22) Pradhan, S.; Hansen, A.; Chakrabarti, B. K. Failure processes in elastic fiber bundles. *Rev. Mod. Phys.* **2010**, *82* (1), 499−555.

(23) Hidalgo, R. C.; Kun, F.; Herrmann, H. J. Creep rupture of viscoelastic fiber bundles. *Phys. Rev. E* **2002**, *65* (1), 106−126.

(24) Kloster, M.; Hansen, A.; Hemmer, P. C. Burst avalanches insolvable models of fibrous materials. *Phys. Rev. Lett.* **1997**, *56* (3), 2615−2625.

(25) Zapperi, S.; Ray, P.; Stanley, H. E.; Vespignani, A. Avalanches in breakdown and fracture processes. *Phys. Rev. E* **1999**, *59* (5), 5049−5057.

(26) Baro, J.; Corral, A.; Illa, X.; Planes, A.; Salje, E. K. H.; Schranz, W.; Soto-Parra, D. E.; Vives, E. Statistical Similarity between the

Compression of a Porous Material and Earthquakes. *Phys. Rev. Lett.* **2013**, *110* (8), 088702.

(27) Hemmer, P. C.; Hansen, A.; Pradhan, S. Rupture processes in fiber bundle models. *Modeling Critical and Catastrophic Phenomena in Geoscience. Springer Berlin Heidelberg.* **2006**, *70S*, 27−55.

(28) Pradhan, S.; Hansen, A.; Hemmer, P. C. Crossover behavior in failure avalanches. *Phys. Rev. E* **2006**, *74* (2), 016122.

(29) Pradhan, S.; Hansen, A.; Hemmer, P. C. Crossover behavior in burst avalanches: Signature of imminent failure. *Phys. Rev. Lett.* **2005**, *95* (12), 125501.